remote sensing

MDPI

Article

Where the Hills Slide Slowly: A LiDAR-Based Morphometric Framework for Landslide Instability Regimes in Soft-Rock Terrains

Szabolcs Kósik [1,*] and Callum Rees [2]

[1] Horizons Regional Council, 10-15 Victoria Avenue, Palmerston North 4410, New Zealand
[2] School of Agriculture and Environment, Massey University, Private Bag 11 222, Palmerston North 4442, New Zealand; c.rees@massey.ac.nz
* Correspondence: szabolcs.kosik@gmail.com

Highlights

What are the main findings?

- Landslide development in the eastern Tararua District is governed by lithologic susceptibility and fluvial incision rather than by slope gradient alone.
- LiDAR-derived morphometrics integrated with geological data discriminate three distinct slope–relief regimes and reveal strong hillslope–channel coupling.

What are the implications of the main findings?

- Assessing the intrinsic susceptibility of rock types and geomorphic parameters independently allows for improved sediment source and hazard interpretation.
- A threshold-based conceptual model integrating lithology, topographic forcing, and land-cover modulation advances remote sensing applications for regional instability assessment in soft-rock terrains.

Abstract

Deep-seated landslide complexes are widespread in soft-rock hill-country landscapes, yet their regional morphometric organisation and controlling factors remain insufficiently quantified. This study uses high-resolution (1 m) airborne LiDAR-derived terrain data integrated with geological and drainage-network datasets to investigate landslide complexes in the eastern Tararua District, New Zealand. A relative, unit-based morphometric framework is applied to compare terrain derivatives (including slope, aspect, and multi-scale relative relief) between mapped landslides and their host geological units. To isolate intrinsic lithological controls from geomorphic influences, the analysis is restricted to landslides occurring entirely within a single geological unit. The results indicate that lithology exerts first-order control on landslide morphometry, while fluvial incision and valley confinement regulate landslide initiation and persistence. Landslides are preferentially associated with low- to mid-order channels, indicating strong hillslope–channel coupling within a young, actively uplifting landscape. A conceptual threshold framework is proposed, showing that landslides develop where lithological susceptibility and relief amplification jointly exceed stability thresholds. By integrating geological information with LiDAR-based morphometric analysis, this study provides a transferable framework for distinguishing instability regimes and improving understanding of sediment dynamics and landscape evolution in soft-rock terrains.

Keywords: deep-seated landslides; earthflows; LiDAR; soft-rock hill country; morphometry; hillslope–channel coupling; lithologic control

Check for updates

Academic Editor: Michele Saroli

Received: 10 March 2026
Revised: 4 April 2026
Accepted: 9 April 2026
Published: 11 April 2026

Copyright: © 2026 by the authors. Licensee MDPI, Basel, Switzerland. This article is an open access article distributed under the terms and conditions of the Creative Commons Attribution (CC BY) license.

1. Introduction

Landslides are widespread geomorphic processes that affect both natural and built environments. Their impacts range from long-term terrain evolution to acute, high-impact disasters. Globally, numerous events highlight their destructive capacity [1–4]. At broader temporal and spatial scales, landslides contribute significantly to the denudation and sculpting of mountainous terrain and landscapes [5,6].

Landslide classifications [7–9] are widely used to describe landslides based on material (rock, debris, or earth) and movement type, such as falls, slides, spreads, and flows. In addition to these categories, the term deep-seated landslide is commonly applied to failures with rupture surfaces extending into bedrock [10,11]. When these deep-seated failures occur in weak, weathered, or poorly lithified "soft rock," they often form large landslide complexes that can persist and reactivate over long periods of time [12–15].

The term stability is commonly used to describe the likelihood of slope failure. Slopes are considered stable when resisting forces exceed driving forces, and unstable when driving forces dominate [16]. The controls on slope stability are commonly grouped into preconditioning, preparatory, triggering, and sustaining factors [17]. Preconditioning factors govern long-term susceptibility and include bedrock strength and structural configuration. Preparatory factors progressively reduce stability, such as uplifting, weathering, or vegetation removal. Triggering factors act over short timescales, with earthquakes and intense rainfall being the most common causes for both shallow and deep-seated failures. In soft rock terrains, rainfall-induced increases in groundwater levels and pore-water pressure are particularly important, often resulting in delayed responses relative to storm events [18]. Sustaining factors influence post-failure behaviour, including continued toe erosion by rivers or coastal processes, and seasonal fluctuations in groundwater pressure [15,19].

Landslides are widespread across the hill-country terrains of New Zealand's North Island, where large areas are underlain by weak Neogene sedimentary rocks prone to deep-seated instability [20–22]. These deep-seated landslides can be long-lived and slow-moving features that are highly sensitive to hydrological, geomorphic and land use change. They shape local landscapes while also affecting pastoral farming [23,24] and pose ongoing hazards to communities and critical infrastructure [25–27]. They also contribute significantly to sediment production, with research showing that a single landslide can deliver up to ~40 kt of sediment to a river system per year [14]. These impacts highlight the need to improve our understanding of landslide susceptibility, behaviour and geomorphology to support sediment source and hazard mitigation.

Our study focuses on deep-seated landslides in the eastern Tararua District, New Zealand (Figure 1). These include planar to rotational slides and earthflows that can be slow-moving and subject to reactivation. To address our research questions, we adopted a data-driven geomorphic interpretation, viewing landslides as landforms shaped by both bedrock properties—expressed as material-strength contrasts (lithology-dependent behaviour)—and external landscape drivers, including slope position, relative relief, and drainage interactions. Bedrock and terrain influences were evaluated within a consistent spatial framework combining regional geological mapping with high-resolution LiDAR-derived topography. Unlike traditional approaches that rely on absolute slope or lithology-based comparisons, this study evaluates landslide morphometry relative to the background terrain within individual geological units, enabling identification of deviations from unit-scale conditions. This approach is used to assess how lithology and terrain morphology influence landslide geometry and surface expression across the study area.

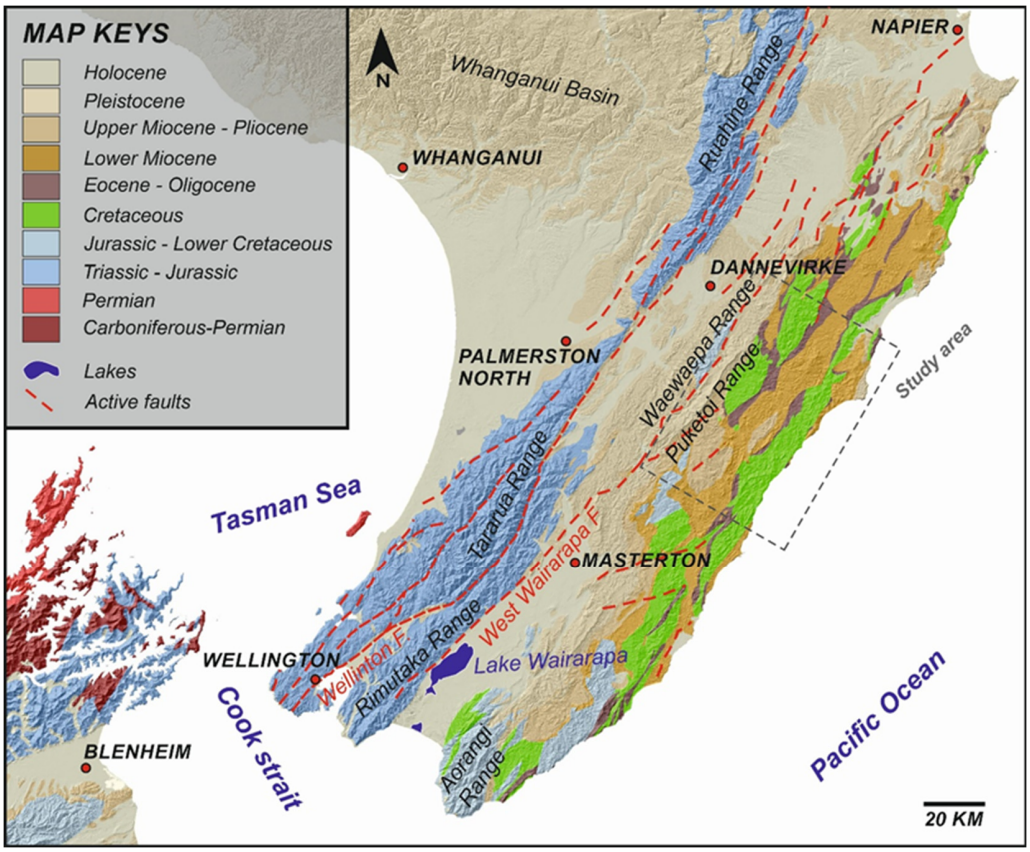

Figure 1. Simplified geology, topography and location of the study area within the lower North Island of New Zealand.

The core objectives of the work were to (1) document and describe morphometric variability within different geological units, (2) test whether the observed morphological contrasts represent structured, interpretable geomorphic domains rather than random scatter, (3) evaluate how morphometric classification relates to geomorphic controls on landslide development and organization, and (4) assess the implications of these patterns for hillslope–channel coupling and sediment transfer in landslide-dominated catchments.

By reframing landslide geometry as a measurable, geologically modulated signal, this study contributes to our understanding of landslides beyond simple mapped boundaries. In particular, the use of relative, unit-based morphometric deviation metrics allows the identification of distinct geomorphic control regimes that are not captured by conventional slope–lithology analyses. This approach facilitates insights into the long-term coupling between geology, terrain, and persistent hillslope instability within a rapidly evolving young landscape.

2. Study Area

The study area is located in the eastern uplands of the Tararua District in the lower North Island of New Zealand (Figure 1). It extends east from the Waewaepa and Puketoi ranges towards the coast, where the Wainui, Ākitio and Aohanga rivers discharge into the Pacific Ocean, forming the main sediment transport routes (Figure 2).

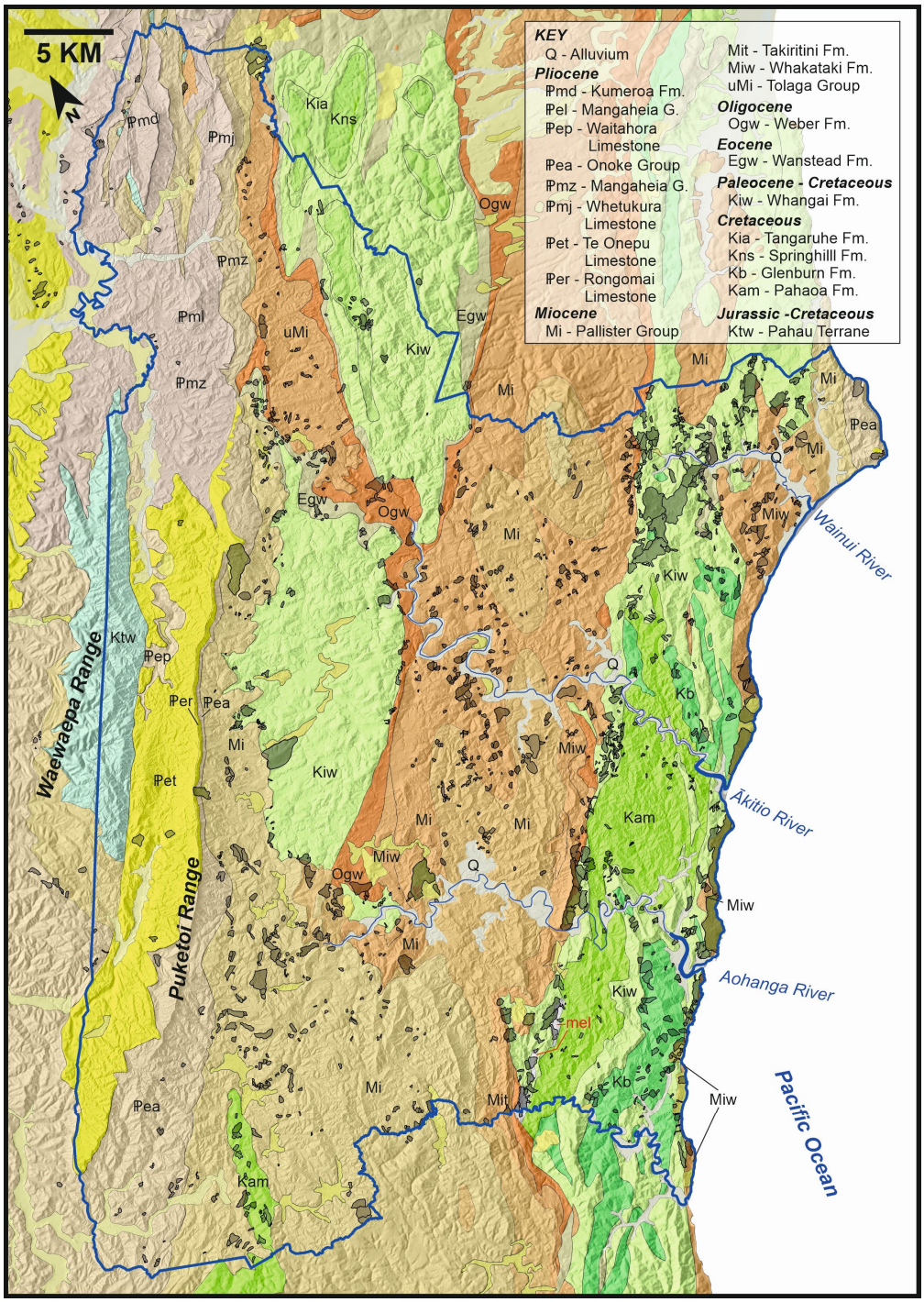

Figure 2. Bedrock geology of the study area (blue outline) with superficial deposits omitted [28]. Landslides mapped in this study are shown as transparent black polygons over a shaded-relief map. Holocene river alluvium (Q) and mélange units (mel) are labelled. Pre-Quaternary geological formations are grouped by age (Jurassic to Pliocene) and coloured accordingly.

This region occupies a forearc position relative to the Hikurangi Subduction Zone, where the Pacific Plate subducts beneath the Australian Plate [29–31]. This tectonic setting exerts a primary control on the geology and structure of the area. Deformation since the early Miocene (~25 Ma) has produced a complex network of west-dipping thrust faults and associated folding [28,29]. Major onshore faults trend northeast-southwest, parallel to the subduction zone, and strongly influence the present-day landscape.

The area is underlain by a partly inverted Cretaceous–Cenozoic marine forearc basin that has been uplifted and deformed by tectonic processes operating along the Hikurangi Subduction Zone. Quaternary landscape evolution in the Tararua District reflects the interplay of tectonic uplift, river incision and aggradation, sea-level fluctuations, and loess deposition [28,32–39], resulting in a complex assemblage of river terraces, uplifted marine surfaces, and rapidly eroding hill-country terrain.

The Waewaepa and Puketoi ranges dominate the landscape, rising up to 800 m above sea level to form the western boundary of the study area. The Waewaepa Range is a fault-bounded block of Mesozoic greywacke and argillite of the Pahau Terrane, flanked by westward-dipping Miocene sedimentary rocks. The Puketoi Range forms a prominent northeast-southwest trending dip slope and escarpment of Pliocene to early Pleistocene limestone interbedded with sandstones and siltstones of the Onoke Group. Between the Puketoi Range and the coast, the landscape comprises deeply incised hill country with common landslides (Figure 2) [28].

3. Data and Methods

3.1. LiDAR Data and Landslide Mapping

The one-metre-resolution bare-earth Digital Elevation Model (DEM) used in this study was derived from an airborne LiDAR survey commissioned and funded by Regional Software Holdings Limited (RSHL) on behalf of the New Zealand Government, with data acquisition and related services contracted to Woolpert NZ Ltd. (Napier, New Zealand) [40]. The LiDAR data were acquired using a Leica Terrain Mapper-2 sensor mounted on a Cessna 402B fixed-wing aircraft, flown at an altitude of approximately 2100 m above ground level. Data acquisition took place between 26 January and 5 May 2024, with an emitted pulse density of approximately 8 pulses per square metre. The resulting DEM is projected in New Zealand Transverse Mercator 2000 (NZTM2000) and referenced vertically to the NZVD2016 datum, with a reported horizontal accuracy of $\pm$1.0 m and vertical accuracy of $\pm$0.2 m at the 95% confidence level.

To support morphometric and terrain interpretation, terrain derivatives including slope, aspect, and relative-relief metrics were generated from the LiDAR-derived DEM using ArcMap 10.4 [41,42]. Landslides were manually delineated using slope and shaded-relief rasters following established geomorphic mapping principles [43,44]. Only large-scale mass movements exhibiting evidence of tension cracks, internal deformation, pressure ridges, and complex accumulation zones were included in this study. Shallow soil slips not displaying these features were excluded from the landslide dataset. Delineation and surface-texture validation were supported using Horizons Regional Council's orthorectified aerial photography from 2016 and 2021 (0.3 m ground resolution; optical bands), consistent with minimum mapping resolutions recommended for landslide interpretation [45]. Mapping was also informed by the multi scale (1:5000–1:250,000) New Zealand National Landslide Database [21], the 1:50,000 Erosion Risk North Island dataset [46], the 1:63,360 1st edition of the New Zealand Land Resource Inventory (NZLRI) for Southern Hawkes Bay-Wairarapa [13,47], and partial coverage of 1:8000 LUC) mapping from the Horizons Regional Council Sustainable Land Use Initiative (SLUI) [48,49]. The principal sources of uncertainty for landslide identification in this study include (1) omission of highly degraded or older landslide features with subdued geomorphic expression, (2) ambiguity in distinguishing the boundaries between deep-seated landslides and adjacent shallow soil-slip-affected terrain, where transitional slope deformation is common, and (3) limited ground truthing and coverage of farm-scale data. These uncertainties are expected to have limited influence on the regional-scale morphometric patterns assessed in this study.

3.2. Geological Data

Bedrock and terrain influences were evaluated using geological units from the 1:250,000 QMAP geological dataset [28], together with a one-metre-resolution LiDAR DEM. In contrast to the high-resolution terrain data, the geological units used in this study are at a broad regional scale and do not capture detailed hillslope scale variability or lithological boundaries, introducing uncertainty into the spatial relationship between individual landslides and lithological boundaries. Regional-scale (1:250,000) fault and structural datasets were not used in this study because they do not adequately capture the density of minor faults and geomorphically expressed structures identifiable in high-resolution LiDAR-derived DEMs [28]. Structural influences are therefore considered conceptually rather than through explicit spatial fault datasets. Because many faults coincide with geological unit boundaries, several analyses were restricted to single-lithology landslides to minimise ambiguity associated with lithologic contacts and potentially structurally controlled (fault-related) boundaries. The role of structural controls may be revisited as higher-resolution fault datasets become available for the Tararua area [50].

3.3. Morphometric Analysis

Relative relief was evaluated at multiple spatial scales (50, 100, and 200 m window sizes) to assess sensitivity to analysis scale. Smaller windows (50 m) emphasised microtopographic variability and produced noisy relief patterns, whereas larger windows (200 m) overly smoothed terrain and obscured hillslope-scale variability associated with landslide morphology. A 100 × 100 m window provided the most consistent representation of hillslope-scale relief relevant to landslide systems and was therefore adopted for subsequent analyses. To ensure statistically robust treatment of circular data, aspect values were analysed using vector components rather than linear averaging. East–west (cosine) and north–south (sine) aspect components were calculated for each grid cell and summarised within analysis units by computing mean vector components. Median aspect direction and directional concentration were then derived from these components using circular statistics, with the resultant vector length used as a measure of orientation strength. Aspect distributions were analysed for the full landslide inventory and for subsets defined by lithology and morphometric cluster.

3.4. Statistical and Clustering Analysis

Morphometric variability among geological units was analysed in Microsoft Excel, with group-level differences assessed using non-parametric statistical approaches implemented in Python 3.10, including Kruskal–Wallis tests to evaluate inter-group contrasts [51]. Where significant differences were identified, post hoc pairwise comparisons were performed using Dunn's test with Bonferroni correction for multiple comparisons [52]. K-means clustering was applied to explore structure and similarity within the multidimensional morphometric dataset [53,54]. The number of clusters (k = 3) was selected based on a combination of silhouette analysis and interpretability, with lower silhouette scores obtained for alternative k values, reflecting the inherently diffuse boundaries of continuous terrain datasets. This combined approach enabled comparison of terrain-controlled morphological variation across contrasting geological settings. To distinguish geology-controlled, mixed-control, and topography-controlled regimes, deviation thresholds of $\pm 2^{\circ}$ for slope and ± 2 m for relative relief were applied to the difference between landslide median values and corresponding geological-unit median values. These thresholds were selected to represent geomorphically meaningful deviations from background terrain conditions rather than statistical outliers. In the single-lithology subset, $\pm 2^{\circ}$ corresponds to approximately 0.7 standard deviations of slope deviation and ± 2 m to approximately

0.3 standard deviations of relief deviation, capturing departures from unit-scale terrain while avoiding over-sensitivity to minor variability.

The selected thresholds represent a balanced sensitivity between meaningful geomorphic variation and minor fluctuations in terrain metrics. Small variations in threshold values would be expected to affect individual classifications locally but are unlikely to alter the overall classification structure or the regional patterns identified.

To evaluate the spatial relationship between landslide occurrence and drainage-network attributes, each landslide polygon was spatially associated with its nearest stream segment from the 30 m River Environment Classification (REC2, 1:50,000) [55]. Stream order was assigned using the Strahler classification scheme [56], and the order of the nearest stream segment was recorded for each landslide polygon. Observed landslide–stream associations were normalised against the distribution of stream orders across the study area to account for the spatial imbalance in stream-order frequency. Expected stream-order frequencies were calculated using the total length of stream segments per order across the entire study area, providing a measure of channel availability. Observed landslide frequencies were then expressed as observed/expected ratios to identify over- or under-representation relative to random expectation. This normalisation was applied to both the full landslide inventory and separately to morphometric landslide clusters, allowing assessment of process-dependent differences in channel coupling while minimising bias related to drainage-network topology.

A comprehensive flowchart summarising the methodological framework is presented in Supplementary Figure S1.

4. Results

4.1. Landslide Inventory—Spatial Distribution

A total of 1587 individual landslide polygons were mapped, covering 104 km^2, equivalent to 5.3% of the study area (Figure 2). The most landslide-prone areas—where landslides cover between 10 and 22% of the land surface—are characterised primarily by mudstone and secondary sandstone lithologies, with ages ranging from Late Cretaceous to the Miocene (~100 to 15 Ma) (Table 1). Only six geological units had no recognised landslides, and together these account for just 3.6% of the study area. These units include relatively competent Pliocene limestones associated with the Puketoi Range and Mesozoic greywacke-argillite of the Waewaepa Range, both of which tend to form stable landscape units within the study area (Figure 1, Table 1).

Table 1. Lithological units and associated landslide abundance, areal extent, and terrain metrics in the study area. The spatial distribution of lithologies and formation names are shown in Figure 2. Lithological unit descriptions follow the Geological Map of the Wairarapa Area and the QMAP 1:250,000 Geological Map of New Zealand [28,57].

Unique Code	Main Rocks	Age (Ma)	Median Relief (m)	Median Slope (Degrees)	Total Area (ha)	Landslide Count	Landslide Area (ha)	Landslide Area (% of Lith. Unit)
24 Pmd	Sandstone (limestone)	1.6–2.4	132	18.5	805.5	1	0.4	0.05
25 Pmv	Mudstone (sandstone, limestone)	1.6–2.4	182	15.5	7.1	0	-	-
20 Pml	Limestone (sandstone)	1.6–5.3	131	18.9	504.5	0	-	-
6 Pep	Coquina (limestone)	1.8–2.6	116	20.4	955.3	0	-	-
2 Pea	Mudstone (sandstone, conglomerate)	2–5.3	144	24.5	11,988.4	40	222.7	1.86
21 Pmz	Sandstone (siltstone, limestone)	2.4–3.6	92	16.6	11,412.1	9	38.1	0.33
22 Pmj	Limestone (sandstone)	2.4–3.6	135	19.7	895.1	0	-	-
1 Pet	Coquina (sandstone, siltstone)	2.5–3.5	155	20.5	11,410.1	8	46.4	0.41
30 Pek	Coquina (limestone, sandstone)	3.6–5.3	156	18.5	12.8	1	0.3	2.30
31 Pmz	Sandstone (mudstone, conglomerate)	3.6–5.3	108	20.3	4990.2	5	64.6	1.29
12 Per	Coquina (limestone, sandstone)	4–4.6	154	22.8	927.0	2	12.0	1.30
26 MI	Sandstone (mudstone, limestone)	3.6–10.9	103	18.5	1288.9	4	25.9	2.01
3 Ms	Conglomerate (sandstone, mudstone)	5–7	123	26.2	636.7	0	-	-
4 Mi	Mudstone (sandstone, congl., tuff)	5.5–11	110	20.4	31,017.5	294	1451.0	4.68

Table 1. *Cont.*

Unique Code	Main Rocks	Age (Ma)	Median Relief (m)	Median Slope (Degrees)	Total Area (ha)	Landslide Count	Landslide Area (ha)	Landslide Area (% of Lith. Unit)
27 uMi	Sandstone (mudstone, limestone)	10.9–25.2	80	15.1	5928.3	73	305	5.15
18 Mi	Mudstone (sandstone, limestone, congl.)	11–16.3	106	19.3	17,159.8	163	712.2	4.15
16 Miw	Sandstone (mudstone, limestone, congl.)	15–24	121	17.1	6404.4	115	1028.1	16.05
19 Mi	Sandstone (mudstone, conglomerate)	16–24	104	17.8	18,980.6	300	1238.6	6.53
11 Mit	Algal limestone (sandstone, mudstone)	16.5–19	143	19.5	213.4	2	139.2	65.23
14 Mit	Sandstone (mudstone, limestone)	16.5–19	192	28.5	706.3	8	54.7	7.75
13 Ogw	Mudstone (marl, sandstone, limestone)	22–42.5	86	13.1	5636.3	86	340.4	6.04
23 Kiw-Og.	Mudstone (sandstone, marl)	22–82	113	16.4	1318.6	36	293.9	22.29
28 Egw	Mudstone	33.7–55	92	13.6	2580	100	349.8	13.56
17 Kiw	Mudstone (sandstone)	58–82	119	18.0	29,752.2	446	3023.9	10.16
10 Kia	Sandstone (mudstone)	65–100	122	19.7	803.4	8	12.3	1.53
9 Kiw	Mudstone (sandstone)	65–99	137	22.8	7643.3	26	82.7	1.08
15 Kb	Sandstone (argillite, mudstone, congl.)	80–100	147	21.5	5735.2	113	636.6	11.10
8 Kns	Mudstone (sandstone, congl., tuff)	95–103	115	19.0	928.4	12	34.8	3.75
5 Ktw	Greywacke (sandstone, mudstone)	98–180	173	29	4027.4	0	-	-
7 Kam	Sandstone (mudstone, argillite, congl.)	100–124	126	24.4	11,019	107	370.1	3.36
29 Ktw	Sandstone (mudstone)	100–146	155	22.1	128.5	1	0.7	0.54

4.2. Terrain Metrics of Mapped Landslides

Landslide areas span more than three orders of magnitude, from <0.2 ha to >230 ha. Median polygon area is 2.9 ha, with 75% landslides smaller than 6.2 ha and 90% smaller than 12.6 ha. A small number of large composite systems exceed 100 ha and strongly influence the mean (6.6 ha). Planform geometry also spans a wide range of scales, with median lengths of ~300 m (interquartile range 202–436 m) and widths of ~155 m (104–234 m). Aspect ratios (width-to-length) cluster mainly between ~0.4 and 0.7, indicating predominantly moderately elongate forms, although rare valley-confined systems extend for >4 km and display highly elongate geometries. The strongly right-skewed distributions of area, length and width indicate that the inventory is dominated numerically by small to moderate landslides, while a limited number of large composite systems define the upper tail of the size spectrum.

The general slope and relative-relief characteristics of the landslides were analysed using histograms of lower (Q1), median (Q2), and upper (Q3) quartiles calculated for each polygon. All quartile metrics display broadly unimodal distributions with systematic shifts towards higher values from Q1 to Q3 (Figure 3). Lower-quartile slopes are concentrated mainly between ~10 and 17°, median slopes peak at ~16–23°, and upper-quartile values shift towards steeper terrain of ~22–33°, with a tail extending to ~40°. Relative-relief distributions show a comparable progression, with Q1 clustering at ~21–41 m, Q2 peaking near ~30–45 m, and Q3 increasing to ~35–55 m and locally exceeding 70 m (Figure 3). Collectively, these quartile-based metrics indicate that the landslides typically occupy strongly rolling to moderately steep, low- to moderate-relief hillslopes but contain substantial internal topographic variability, consistent with composite morphologies characterised by gentler depositional lobes downslope and steeper, more incised source areas upslope or, in some cases, extensive backscarps.

Slope gradient and relative relief distribution have been assessed for all individual landslide polygons, along with the aspect distributions for each lithological unit. Median relative relief and median slope show systematic variation among lithological groups (Figure 4). When considering the full inventory and mixed-lithology polygons, landslides typically occupy moderate-relief terrain (median values ~35–42 m) and moderately steep slopes (~18–21°). Several individual geological units deviate from these central tendencies. Some of the units dominated by older Cretaceous to Paleocene (~56–100 Ma) mudstone–sandstone successions (e.g., Kiw, Kam) display elevated median relative relief and steeper median slopes, indicating preferential development on more dissected hillslopes. In contrast, some younger Oligocene to Eocene (~23–42 Ma) (or more weakly

dissected units (e.g., Ogw) exhibit lower relief and gentler slopes. Interquartile ranges differ substantially between lithologies, indicating contrasting degrees of internal morphometric variability. Outliers are present across most lithological units and include both unusually steep and unusually low-relief settings (Figure 4). Together, these patterns demonstrate that landslide morphometry is unevenly distributed across geological units rather than uniformly expressed across the landscape.

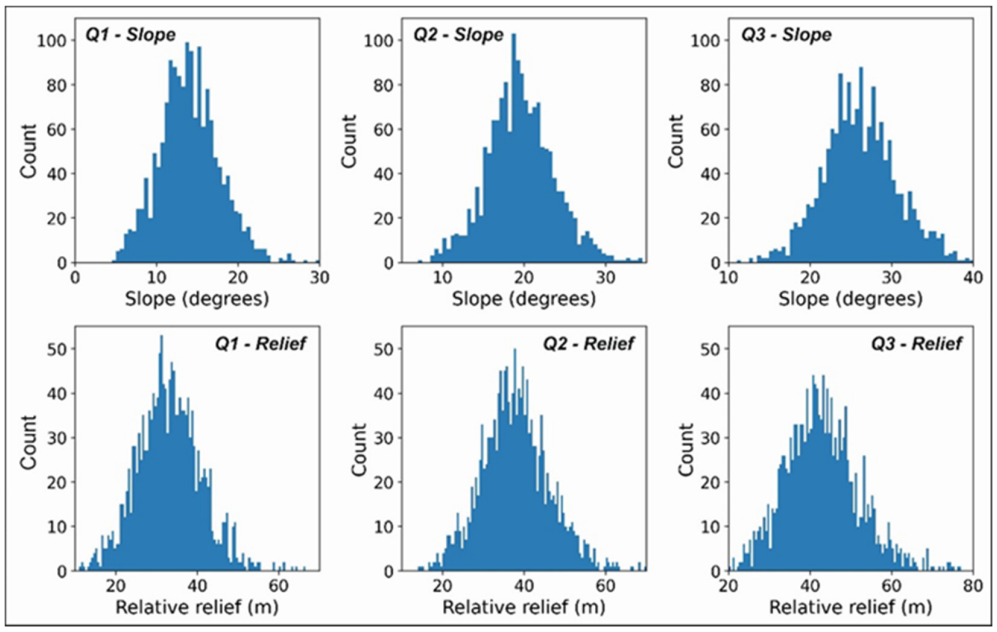

Figure 3. Quartile histograms (Q1, Q2, Q3) of slope and relative relief calculated for mapped landslide polygons from the 1 m LiDAR-derived DEM.

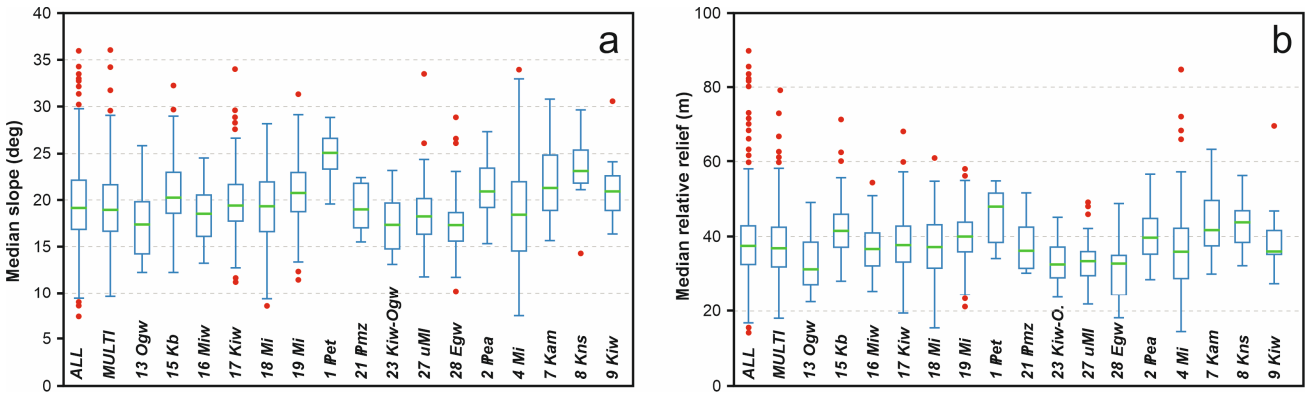

Figure 4. Box-and-whisker plots of median landslide slope (**a**) and median relative relief (**b**). "ALL" represents the full population of mapped landslides, while "MULTI" denotes landslides intersecting more than one lithological unit. Remaining boxes show landslides confined to a single lithology (Table 1). Whiskers extend to 1.5× the interquartile range (red dots) indicate statistical outliers.

Landslide aspect varies systematically between lithological units (Figure 5). No single regional preferred flow direction is evident across the study area. Some of the lithologies (Kiw and Mi units) exhibit broad, multimodal directional patterns, reflected in low resultant vector lengths (R) and high circular dispersion values. In contrast, the Kb and Kam units show more concentrated aspect distributions, with mean vector directions clustering within the SE–S–SW sectors and comparatively higher R values. Across most lithological units, north to northwest (N–NW) orientations are weakly represented or absent in the rose diagrams. Overall, aspect distributions differ between geological units in both dominant orientation and degree of directional concentration.

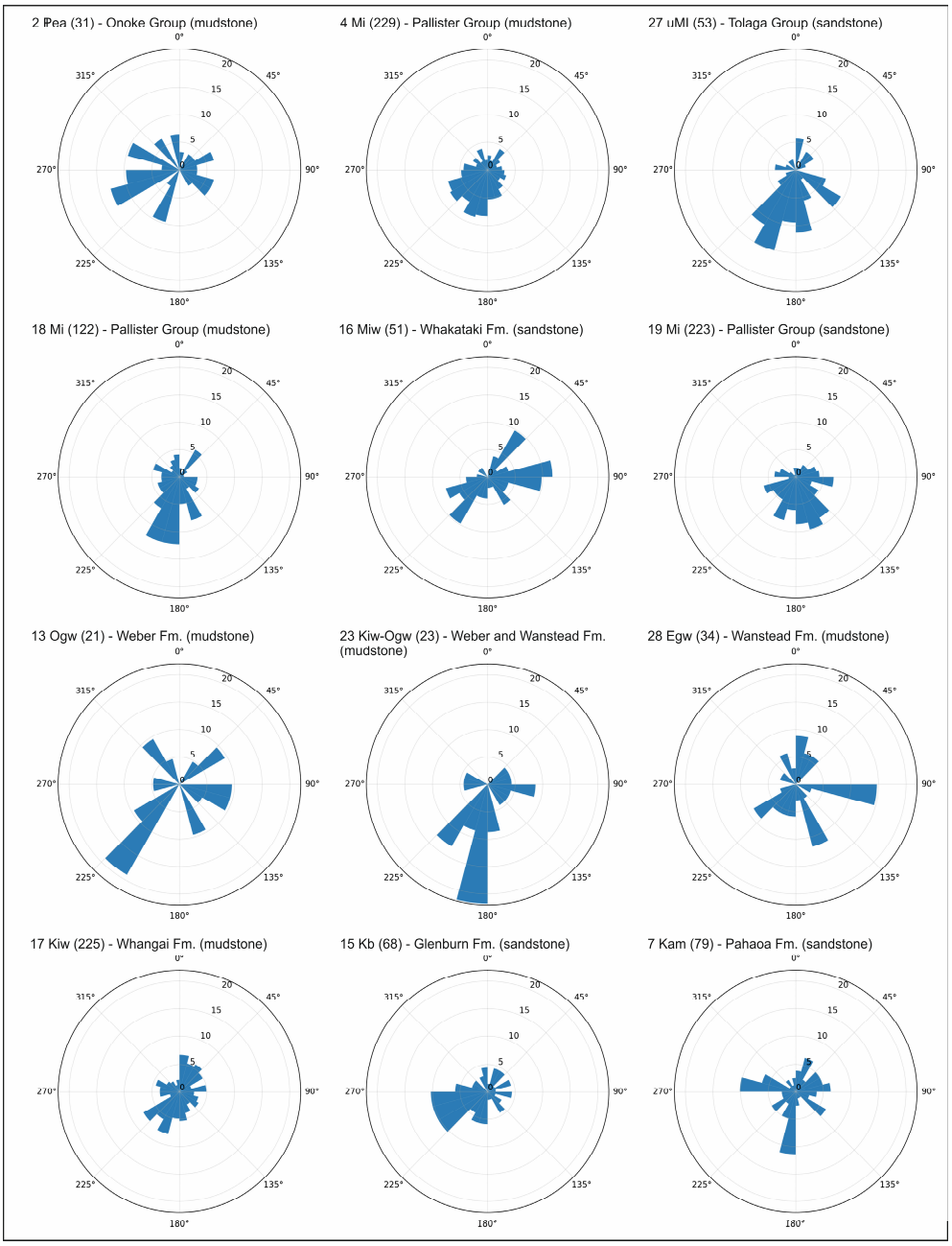

Figure 5. Rose diagrams of landslide median aspect for the 12 lithological units containing the highest number of mapped landslides (sample size, *n*, in brackets), using 15° directional bins. Lithologies are arranged stratigraphically according to the minimum age of each unit, from youngest (**top-left**) to oldest (**bottom-right**). Radial values represent the percentage of landslides per directional bin. All panels are plotted on a uniform radial scale (maximum = 22%) to allow direct comparison of directional strength and dispersion between lithological units.

4.3. Lithological Controls on Landslide Morphology

To assess whether lithology exerts a measurable control on landslide occurrence and associated morphometric conditions, the median slope and median relative relief of landslides were compared with those of their enclosing geological units for single-lithology cases. Restricting the analysis to single-lithology landslides (n = 1202) minimises boundary effects and isolates intrinsic within-unit morphometric behaviour. The magnitude of deviation between geological-unit median slope and landslide median slope varies among lithologies, and a comparable pattern is evident for median relative relief. Units dominated

by Pea, Mi, and Kam display comparatively lower median slope deviations, whereas Ogw and Egw units exhibit higher deviations (Figure 6). To evaluate whether these differences are statistically significant, a Kruskal–Wallis H-test was applied to the slope deviation values [56]. The test yielded a highly significant result ($H = 294.1$, $p < 0.001$), confirming that slope deviations differ systematically among geological units.

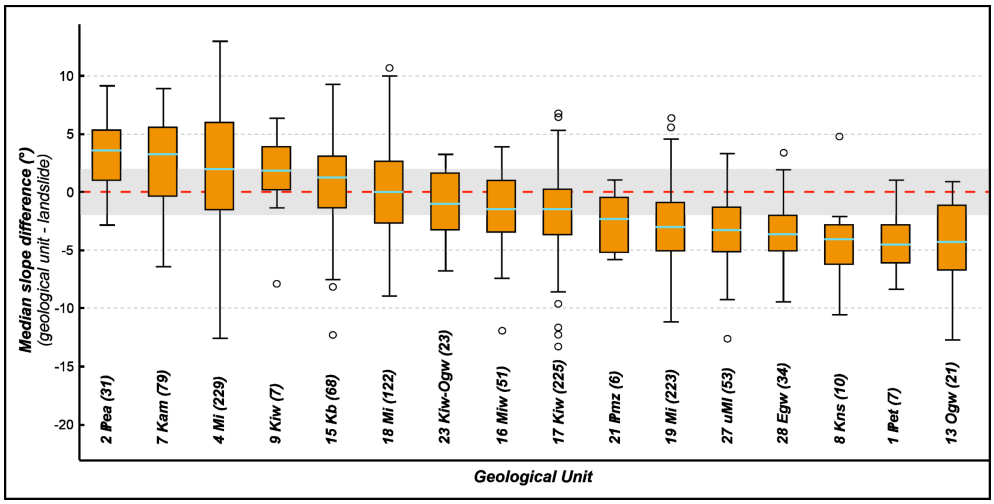

Figure 6. Box-and-whisker plot showing slope differences for landslides that fall entirely within a single geological unit. Values represent the difference between the median slope of the geological unit and the median slope of the landslides contained within that geological unit. Sample sizes (n) for each unit are shown after each label in brackets. The grey band indicates the $\pm 2^{\circ}$ threshold used for classification in the conceptual model.

Post hoc pairwise comparisons using Dunn's test with Bonferroni correction show that significant differences are limited to specific lithological contrasts rather than being uniformly expressed across all units. Detailed results are provided in Supplementary Figure S2.

4.4. Morphometric Classification of Landslides

To identify recurring slope–relief patterns in landslide morphology and assess whether these patterns form statistically distinct geomorphic groupings, we applied an unsupervised clustering approach. Landslide polygons were classified into geomorphically distinct groups using a k-means clustering method applied to median slope and relief quartiles [53]. A three-cluster solution was selected based on cluster separation and interpretability, supported by a silhouette score of 0.43 [58], indicating a moderately well-defined grouping structure for what is inherently continuous landscape data. The three clusters represent distinct combinations of slope–relief characteristics: Cluster 1 comprises landslides with generally higher slopes and elevated local relief, corresponding to deeply incised terrain or active headwall environments; Cluster 2 contains moderate-slope, moderate-relief landslides typical of broad soft-rock hill country; and Cluster 3 represents lower-slope, lower-relief landslides situated on subdued terrain or in more weathered lithologies (Figure 7). Comparison with mapped geological units shows that weak mudstone and siltstone formations (e.g., Mit, Mi, Kb) are disproportionately represented in the lower-slope/relief clusters, whereas units associated with stronger incision or mixed lithological domains (e.g., Kiw, Ogw) are more prevalent in the high-slope, high-relief cluster.

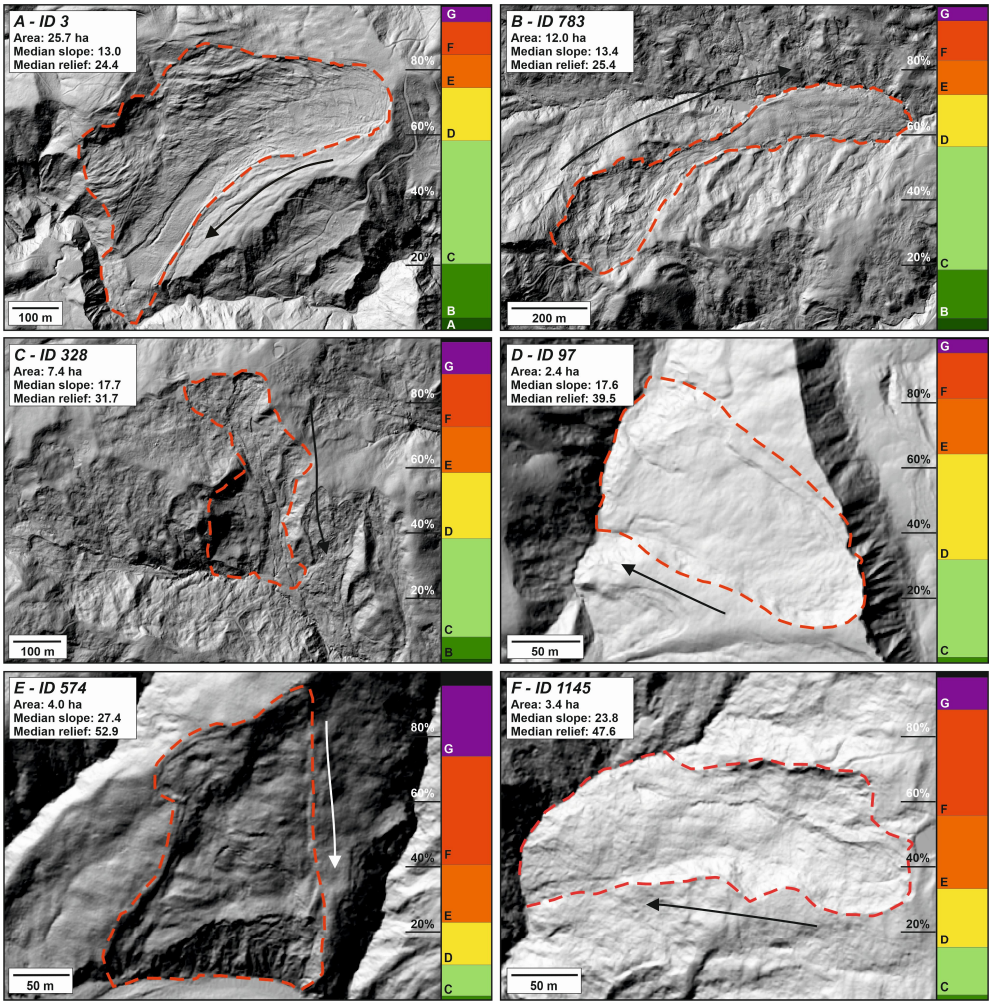

Figure 7. Representative landslides from the study area illustrating low-slope/low-relief (**A**,**B**), moderate-slope/moderate-relief (**C**,**D**), and high-slope/high-relief (**E**,**F**) morphometries. These groups correspond to the three morphometric clusters derived from k-means classification of median slope and relief quartile metrics. Red dashed lines delineate the desktop-mapped landslide boundaries, and black or white arrows indicate inferred downslope movement direction. The colour scale adjacent to each shaded relief map shows slope classes following the Land Use Capability (LUC) system used in New Zealand [47]: A (0–3°), B (3–7°), C (7–15°), D (15–20°), E (20–25°), F (25–35°), and G (>35°). The G class is subdivided into 35–45° (purple) and >45° (black) to emphasise very steep slopes, which commonly correspond to backscarp areas.

4.5. Controls of Channel Hierarchy on Landslide Distribution

To evaluate whether landslide occurrence varies systematically with channel hierarchy (headwaters versus larger waterways), we compared the observed distribution of landslides across Strahler stream orders with the expected distribution based on stream-network availability. The normalised observed/expected ratios reveal a clear stream-order dependence. When all landslides are considered together, first- and third-order streams are slightly over-represented (ratios > 1), whereas second-order streams occur approximately in proportion to their availability (ratio ≈ 1), and higher-order channels show progressively increasing under-representation. Fifth- and sixth-order streams display the lowest ratios (<0.5) (Figure 8). Cluster-specific patterns follow a similar overall trend but differ in magnitude. High-slope/high-relief landslides show peak over-representation in third-order channels (ratio ≈ 1.2), while moderate-slope/moderate-relief landslides are concentrated in first- and third-order streams and decline toward higher orders. Low-slope/low-relief landslides exhibit only slight over-representation in first-order channels

and become strongly under-represented from fourth order onward, particularly in fifth- and sixth-order streams (ratio < 0.3). Across all clusters, stream orders ≥4 consistently show ratios below 1 (Figure 8).

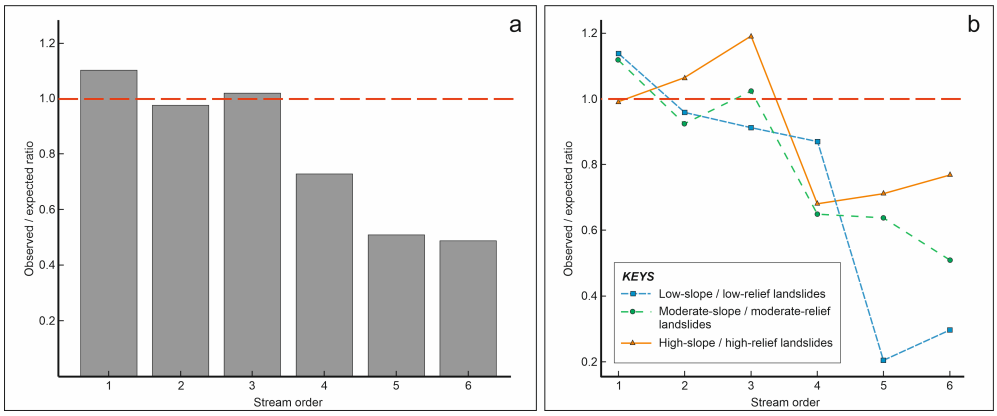

Figure 8. (**a**) Normalised stream-order preference (observed/expected ratio) for all mapped landslides. Ratios represent observed frequency relative to expected frequency based on stream-network distribution. The dashed horizontal line indicates proportional occurrence (ratio = 1). (**b**) Normalised stream-order preference of landslides by morphometric cluster. Values greater than 1 indicate over-representation relative to stream-network availability, whereas values below 1 indicate under-representation. High-slope/high-relief landslides show peak preference in third-order channels, while low-slope/low-relief landslides are strongly under-represented in higher-order streams (orders 5–6). The dashed horizontal line indicates proportional distribution (ratio = 1).

5. Discussion

In general, the type and severity of erosion may be related to a combination of the following factors: regional structure, tectonism, lithology (bedrock and regolith properties, including depth to bedrock), soil properties, slope characteristics (angle, shape, aspect), vegetation cover and climatic conditions [59–65].

Landslide development in the study area reflects the interaction between lithologic properties, topographic forcing, drainage-network organisation, and inherited structural architecture. By integrating morphometrics derived from LiDAR DEMs, clustering analysis, lithology-specific control regimes, and footprint weighting, this study identifies distinct instability regimes within the landscape rather than a simple slope–failure relationship. Similar multi-factor controls on deep-seated and slow-moving landslides have been recognised globally, where landslides emerge from the coupling of lithologic susceptibility, relief amplification, and structural inheritance [66,67].

High-resolution terrain analysis increasingly allows such interactions to be quantified using inventory-based and DEM-derived morphometrics [68]. However, linking terrain metrics explicitly to lithologic and structural domains remains less commonly addressed [69].

5.1. Lithology–Relief Coupling and Morphometric Patterns

The systematic variation in slope, relief, and aspect metrics across geological units confirms that lithology exerts a first-order control on landslide morphology. Geological units dominated by mudstone with high landslide counts (e.g., Mi, Pea) are associated with lower median slopes and reduced slope deviations relative to background terrain, whereas relatively more competent units with high landslide counts (e.g., Kiw, Kam) exhibit steeper and more dissected morphometric signatures. The Kruskal–Wallis yielded a significant result, indicating that these differences are statistically robust and not artefacts of terrain variability. Comparable lithologic controls on landslide geometry and activity

have been documented in the Northern California Coast Ranges, where material strength and weathering state influence both susceptibility and morphometric expression [70,71].

The k-means clustering further shows that landslides occupy structured slope–relief domains rather than forming a continuous morphometric spectrum. Although the silhouette score (0.43) indicates moderate separation—expected for continuous terrain data—the clusters reveal meaningful organisation within slope–relief space. High slope–high relief clusters correspond to deeply incised terrain and probable headscarp-dominated systems, whereas low slope–low relief clusters represent landslides within gentler hill-country settings. These patterns support the concept that slope–relief conditions are emergent properties of lithology–incision coupling. Williams et al. demonstrated that fluvial incision interacting with weak geological structures can produce departures from universal threshold slope models [72]. The results from this study similarly indicate that slope angle alone cannot explain landslide distribution and that fluvial incision and lithology must also be considered. Importantly, restricting the analysis to single-lithology polygons isolates intrinsic unit behavior and reduces boundary artefacts. The persistence of significant morphometric contrasts under this constraint confirms that these patterns are inherent to the geological units themselves. Although not assessed in this paper, the presence and orientation of faults, folds, bedding, fracture zones and jointing and clay mineralogy have been highlighted as important controls in previous work [13,28].

5.2. Directional and Fluvial Controls on Landslide Organisation

Aspect distributions reveal additional lithology-dependent structure. Geological units such as Pea, Kiw and Kam display broad, multimodal aspect patterns and low resultant vector lengths, indicating weak directional confinement, whereas Mi and Kb show more concentrated SE–S–SW orientations. Directional asymmetry in landslide occurrence has been linked to structural grain, hydro-mechanical forcing, and climatic controls [71,73]. The systematic under-representation of N–NW aspects across most lithologies suggests landscape-scale asymmetry in slope exposure or structural alignment. This likely reflects an interaction between regional structural architecture, valley orientation, and drainage-network organisation [22,74,75]. Previous studies in the Wairarapa hill country reported a predominance of landslides on north-facing slopes [65], but those inventories were largely dominated by shallow soil slips triggered during intense rainfall events. In contrast, the present study focuses primarily on deep-seated translational to rotational slides and earthflows, which may respond more strongly to longer-term moisture conditions and sustained hillslope saturation. Consequently, wetter and less isolated south-facing slopes may favour the formation and reactivation of these deeper failures, whereas drier north-facing slopes may be more prone to shallow soil-slip processes during short-duration storm events [65,76,77].

Normalised stream-order analysis indicates that landslides are over-represented in low- to mid-order streams and progressively under-represented in higher-order channels. High slope–high relief systems exhibit a particularly strong preference for third-order streams. This pattern is consistent with strong hillslope–channel coupling in incised headwater and mid-order valleys, where toe erosion and confinement sustain reactivation. In contrast, higher-order rivers typically occupy wider valleys with more extensive floodplains, often resulting in lower connectivity between the channel and adjacent hill slopes. Where wider floodplains occur, the opportunity for the channel to remove toe material, undercut hill slopes, and initiate landslides is reduced [78]. Greater stream power and ability to transport sediment in higher order reaches also means preservation potential of landslide deposits is lower due to stronger channel reworking and lateral erosion. Similar feedback between landsliding and fluvial incision has been documented in the Ruahine Ranges [79] and

in other landslide-dominated terrains [70]. Together, the aspect and stream-order results reinforce that incision depth and valley confinement modulate morphometric expression in conjunction with lithologic susceptibility.

5.3. Landslide Footprint, Control Regimes, and Landscape-Scale Impact

Control-regime proportions describe how landslides behave within each lithology, but they do not directly indicate geomorphic impact. To address this, a lithology-specific landslide footprint was evaluated using the absolute landslide area. When control-space positions are weighted by absolute landslide area, the regional signal is not dominated by the most extreme geology-controlled units but by lithologies that host the largest unstable terrain footprint. Units such as Mi, Miw, Egw and Kiw collectively account for a substantial proportion of total mapped landslide area and tend toward mixed or topography-dominated regimes. This pattern indicates that lithologies with the greatest geomorphic influence are not necessarily those with the highest relative susceptibility, but those that host the largest and most spatially extensive landslides. In this context, landslide frequency alone is not a sufficient indicator of geomorphic significance, as landscape evolution is disproportionately influenced by large, spatially extensive landslide complexes rather than numerous small failures. A similar distinction was noted in California, where large, persistent landslides contribute disproportionately to sediment yield despite occurring within a limited extent of highly susceptible lithologies [70]. It also highlights that landslide frequency and landscape impact are not equivalent metrics—a distinction increasingly emphasised in susceptibility and hazard modelling frameworks [80]. Lithologies with very small outcrop area and disproportionately high percentage coverage (11 Mit) were excluded from weighted synthesis to avoid small-denominator bias, as such cases likely reflect local structural coincidence rather than intrinsic susceptibility.

5.4. Refined Conceptual Model and Implications for Remote Sensing

From a remote sensing perspective, the approach presented here is not limited to the specific geological or geomorphic context of the study area but represents a transferable framework for analysing landslide morphometry using high-resolution topographic data. By combining LiDAR-derived terrain metrics with geological and drainage network information, the method enables quantification of deviations between landslide morphology and background terrain conditions, providing a basis for distinguishing between lithological and topographic controls. This approach is applicable in other regions where high-resolution DEMs and basic geological datasets are available and offers a scalable means of linking remotely sensed terrain data to process-based interpretations of landscape instability.

The results support a refined conceptual model in which landslide development is governed by the interaction of intrinsic geological susceptibility (material weakness, weathering state, anisotropy), topographic forcing (relief amplitude, incision depth, valley confinement). This framework extends classical descriptions of landslides by integrating morphometric classification with stratigraphic differentiation [66]. Within this model, geology-dominated regimes occur where weak materials fail under relatively low to moderate relief; topography-dominated regimes arise where steep incision drives instability even in moderately competent units; and coupled regimes represent terrains where weak lithologies coincide with high relief. Transitional or boundary-influenced units occupy intermediate positions, reflecting modulation by stratigraphic contrasts and inherited tectonic architecture (Figure 9), consistent with litho-structural controls documented earlier [22,72].

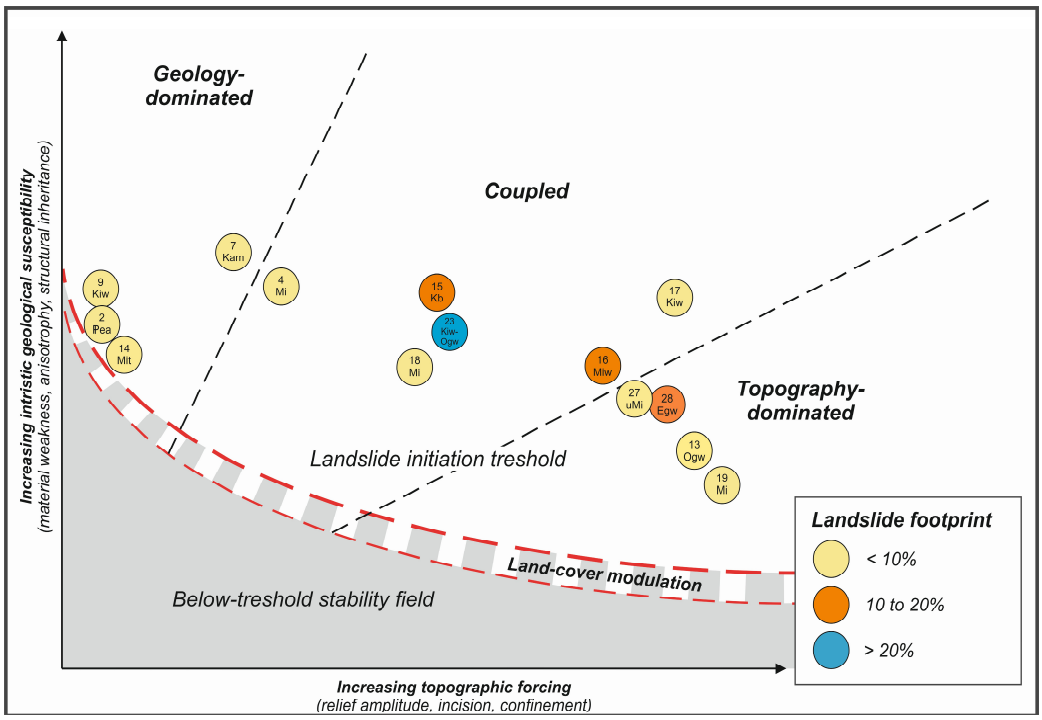

Figure 9. Conceptual model of lithology–topography control on landslide development in the study area. Geological units are positioned according to the dominant control regime expressed by landslides confined to each unit (single-lithology cases), derived from slope and relief deviations relative to host-unit background conditions. The curved boundaries (red dashed lines) represent conceptual landslide initiation thresholds under contrasting land-cover conditions [81], with the upper, thicker curve corresponding to native vegetation and the lower curve to pastoral land use. The shaded field indicates below-threshold stability. Land cover is therefore treated as a threshold modifier rather than an explicit axis, reflecting its role in shifting the initiation envelope without being directly quantified in this analysis.

Structural inheritance will have an influence on landslide development, particularly where faults coincide with lithologic contacts that create zones of mechanical weakness within soft-rock sequences. This influence is not tested in this study, representing a key limitation. Limited field observations and high-resolution mapping in selected parts of the study area indicate that structural controls are locally important, with higher densities of landslides observed along belts of crushed argillite and jointed mudstone identified through farm-scale LUC mapping. As a result, the role of structural control is inferred indirectly rather than quantified explicitly at the regional scale. Future work integrating high-resolution structural datasets derived from LiDAR analysis, including lineament extraction and detailed field mapping, could better resolve the influence of structural inheritance on landslide initiation and evolution.

6. Conclusions

This study presents a quantitative morphometric framework for analysing deep-seated landslides using high-resolution LiDAR-derived terrain data integrated with geological and drainage-network information. The results indicate that landslide morphology reflects the interaction between lithological susceptibility, topographic forcing, and structural influences rather than a single slope-controlled model.

A relative, unit-based analysis demonstrates that landslide morphometry varies systematically across geological units and enables the identification of distinct geomorphic control regimes linked to incision state and terrain organisation. Landslides are preferen-

tially associated with low- to mid-order channels, highlighting strong hillslope–channel coupling and the role of fluvial processes in sustaining long-term instability.

The proposed framework provides a transferable approach for interpreting landslide behaviour using remotely sensed terrain data and improves understanding of sediment dynamics and landscape evolution in soft-rock catchments.

Supplementary Materials: The following supporting information can be downloaded at https://www.mdpi.com/article/10.3390/rs18081135/s1: Figure S1: Methodological workflow of the LiDAR-based morphometric framework; Figure S2: Pairwise comparison matrices for slope and relative relief differences between lithological units.

Author Contributions: Conceptualization, S.K.; methodology, S.K. and C.R.; software, S.K.; formal analysis, S.K.; investigation, writing—original draft preparation, S.K.; writing—review and editing, S.K. and C.R.; visualization, S.K. All authors have read and agreed to the published version of the manuscript.

Funding: This research received no external funding.

Data Availability Statement: The data and materials supporting the findings of this study are available from the corresponding author upon reasonable request.

Acknowledgments: The authors thank Malcolm Todd (Horizons Regional Council) and Alan Palmer (Massey University) for valuable discussions on the geology and landslide characteristics of the Tararua area.

Conflicts of Interest: The authors declare no conflicts of interest.

Abbreviations

The following abbreviations are used in this manuscript:

DEM	Digital elevation model
LUC	Land use capability
NZLRI	New Zealand Land Resource Inventory
NZVD2016	New Zealand Vertical Datum 2016
REC	River environment classification
SLUI	Sustainable land use initiative

References

1. Guzzetti, F. Landslide fatalities and the evaluation of landslide risk in Italy. *Eng. Geol.* **2000**, *58*, 89–107. [CrossRef]
2. Petley, D.N.; Dunning, S.A.; Rosser, N.J. The analysis of global landslide risk through the creation of a database of worldwide landslide fatalities. In *Landslide Risk Management*; Hungr, O., Fell, R., Couture, R., Eberhardt, E., Eds.; CRC Press: London, UK, 2005; pp. 377–384.
3. Yin, Y.; Wang, F.; Sun, P. Landslide hazards triggered by the 2008 Wenchuan earthquake, Sichuan, China. *Landslides* **2009**, *6*, 139–152. [CrossRef]
4. Lapa, R.O.; Bögöly, G. The Vajont Landslide: An overview of 60 years of research. *Rock Mech. Lett.* **2025**, *2*, 160–170. [CrossRef]
5. Korup, O.; Densmore, A.L.; Schlunegger, F. The role of landslides in mountain range evolution. *Geomorphology* **2010**, *120*, 77–90. [CrossRef]
6. Larsen, I.J.; Montgomery, D.R. Landslide erosion coupled to tectonics and river incision. *Nat. Geosci.* **2012**, *5*, 468–473. [CrossRef]
7. Varnes, D.J. Slope movement types and processes. In *Landslides: Analysis and Control*; Schuster, R.L., Krizek, R.J., Eds.; Transportation Research Board, National Academy of Sciences: Washington, DC, USA, 1978; pp. 11–33.
8. Cruden, D.M.; Varnes, D.J. Landslide types and processes. In *Landslides: Investigation and Mitigation*; Turner, A.K., Schuster, R.L., Eds.; Special Report 247; Transportation Research Board, National Research Council: Washington, DC, USA, 1996; pp. 36–75.
9. Hungr, O.; Leroueil, S.; Picarelli, L. The Varnes classification of landslide types, an update. *Landslides* **2014**, *11*, 167–194. [CrossRef]
10. Korup, O.; Clague, J.J.; Hermanns, R.L.; Hewitt, K.; Strom, A.L.; Weidinger, J.T. Giant landslides, topography, and erosion. *Earth Planet. Sci. Lett.* **2007**, *261*, 578–589. [CrossRef]

11. Crosta, G.B.; Frattini, P.; Agliardi, F. Deep seated gravitational slope deformations in the European Alps. *Tectonophysics* **2013**, *605*, 13–33. [CrossRef]
12. Skempton, A.W.; DeLory, F.A. Stability of natural slopes in London clay. In Proceedings of the 4th International Conference on Soil Mechanics and Foundation Engineering, London, UK, 12–24 August 1957; Volume 2, pp. 378–381.
13. Noble, K.E. *Land Use Capability Classification of the Southern Hawke's Bay–Wairarapa Region: A Bulletin to Accompany New Zealand Land Resource Inventory Worksheets*; Land Resources Group, Soil Conservation Centre, Aokautere, Ministry of Works and Development: Palmerston North, New Zealand, 1985; 129p.
14. Massey, C.I.; Petley, D.N.; McSaveney, M.J.; Archibald, G. Basal sliding and plastic deformation of a slow, reactivated landslide in New Zealand. *Eng. Geol.* **2016**, *208*, 11–28. [CrossRef]
15. McColl, S.T.; Holdsworth, C.N.; Fuller, I.C.; Todd, M.; Williams, F. Disproportionate and chronic sediment delivery from a fluvially controlled, deep-seated landslide in Aotearoa New Zealand. *Earth Surf. Process. Landf.* **2022**, *47*, 1972–1988. [CrossRef]
16. Crozier, M.J. *Landslides: Causes, Consequences and Environment*; Croom Helm: London, UK, 1985; 252p. [CrossRef]
17. Glade, T.; Crozier, M.J. The nature of landslide hazard impact. In *Landslide Hazard and Risk*; Glade, T., Anderson, M.G., Crozier, M.J., Eds.; John Wiley & Sons: Chichester, UK, 2005; pp. 41–74.
18. Prokešová, R.; Medveď ová, A.; Tábořík, P.; Snopková, Z. Towards hydrological triggering mechanisms of large deep-seated landslides. *Landslides* **2013**, *10*, 239–254. [CrossRef]
19. Handwerger, A.L.; Huang, M.-H.; Fielding, E.J.; Booth, A.M.; Bürgmann, R. A shift from drought to extreme rainfall drives a stable landslide to catastrophic failure. *Sci. Rep.* **2019**, *9*, 1569. [CrossRef]
20. Pettinga, J.R. Ponui Landslide: A deep-seated wedge failure in Tertiary weak-rock flysch, Southern Hawke's Bay, New Zealand. *N. Z. J. Geol. Geophys.* **1987**, *30*, 415–430. [CrossRef]
21. Rosser, B.; Dellow, S.; Haubrock, S.; Glassey, P. New Zealand's national landslide database. *Landslides* **2017**, *14*, 1949–1959. [CrossRef]
22. Rees, C.; Palmer, A.; Palmer, J. Litho-structural controls on Quaternary landslide distribution in the Rangitikei hill country, North Island, New Zealand. *N. Z. J. Geol. Geophys.* **2020**, *63*, 90–109. [CrossRef]
23. Dellow, S.; Massey, C.I.; McColl, S.; Townsend, D.; Villeneuve, M. Landslides caused by the 14 November 2016 Kaikōura earthquake, South Island. In Proceedings of the 20th NZGS Geotechnical Symposium, Napier, New Zealand, 24–26 November 2016; pp. 1–8.
24. McColl, S.; McCabe, M. The causes and agricultural impacts of large translational landslides: Case studies from North Island, New Zealand. In *Landslides and Engineered Slopes: Experience, Theory and Practice*; Aversa, S., Cascini, L., Picarelli, L., Scavia, C., Eds.; CRC Press: Boca Raton, FL, USA, 2016; pp. 1401–1408.
25. Hancox, G.T. The 1979 Abbotsford landslide, Dunedin, New Zealand: A retrospective look at its nature and causes. *Landslides* **2008**, *5*, 177–188. [CrossRef]
26. Massey, C.I.; Petley, D.N.; McSaveney, M.J. Patterns of movement in reactivated landslides. *Eng. Geol.* **2013**, *159*, 1–19. [CrossRef]
27. McSaveney, M.J.; Massey, C.I. Inadvertent engineered activation of Utiku landslide, New Zealand. In *Advancing Culture of Living with Landslides*; Mikoš, M., Vilímek, V., Yin, Y., Sassa, K., Eds.; Springer International Publishing: Cham, Switzerland, 2017; pp. 563–568.
28. Lee, J.M.; Begg, J.G. *Geology of the Wairarapa Area*; Institute of Geological & Nuclear Sciences 1:250,000 Geological Map 11; 66 p. + 1 folded map; Institute of Geological & Nuclear Sciences Limited: Lower Hutt, New Zealand, 2002.
29. Cole, J.W.; Lewis, K.B. Evolution of the Taupo–Hikurangi subduction system. *Tectonophysics* **1981**, *72*, 1–21. [CrossRef]
30. Nicol, A.; Mazengarb, C.; Chanier, F.; Rait, G.; Uruski, C.; Wallace, L. Tectonic evolution of the active Hikurangi subduction margin, New Zealand, since the Oligocene. *Tectonics* **2007**, *26*, TC4002. [CrossRef]
31. Sutherland, R.; Stagpoole, V.; Uruski, C.; Kennedy, C.; Bassett, D.; Henrys, S.; Davey, F.; Stern, T.; Okaya, D.; Henrys, S.; et al. Reactivation of tectonics, crustal underplating, and uplift after 60 Myr of passive subsidence, Raukumara Basin, Hikurangi–Kermadec fore arc, New Zealand: Implications for global growth and recycling of continents. *Tectonics* **2009**, *28*, TC5017. [CrossRef]
32. Trewick, S.A.; Bland, K.J. Fire and slice: Palaeogeography for biogeography at New Zealand's North Island/South Island juncture. *J. R. Soc. N. Z.* **2012**, *42*, 153–183. [CrossRef]
33. Palmer, J.; Németh, K.; Palmer, A.; Kósik, S. Geoheritage values of the Wairarapa "Mudstone Country", North Island, New Zealand. *Geoconserv. Res.* **2020**, *3*, 129–144. [CrossRef]
34. Pillans, B.J.; Roberts, A.P.; Wilson, G.S.; Abbott, S.T.; Alloway, B.V. Magnetostratigraphic, lithostratigraphic and tephrostratigraphic constraints on Lower and Middle Pleistocene sea-level changes, Wanganui Basin, New Zealand. *Earth Planet. Sci. Lett.* **1994**, *121*, 81–98. [CrossRef]
35. Berryman, K.; Marden, M.; Eden, D.; Mazengarb, C.; Ota, Y.; Moriya, I. Tectonic and paleoclimatic significance of Quaternary River terraces of the Waipaoa River, east coast, North Island, New Zealand. *N. Z. J. Geol. Geophys.* **2000**, *43*, 229–245. [CrossRef]
36. Litchfield, N.; Berryman, K. Relations between postglacial fluvial incision rates and uplift rates in the North Island, New Zealand. *J. Geophys. Res. Earth Surf.* **2006**, *111*, F02008. [CrossRef]

37. Litchfield, N.J. Using fluvial terraces to determine Holocene coastal erosion and Late Pleistocene uplift rates: An example from northwestern Hawke Bay, New Zealand. *Geomorphology* **2008**, *99*, 369–386. [CrossRef]
38. Grant, G.R.; Sefton, J.P.; Patterson, M.O.; Naish, T.R.; Dunbar, G.B.; Hayward, B.W.; Morgans, H.; Alloway, B.; Seward, D.; Tapia, C.; et al. Mid- to late Pliocene (3.3–2.6 Ma) global sea-level fluctuations recorded on a continental shelf transect, Whanganui Basin, New Zealand. *Quat. Sci. Rev.* **2018**, *201*, 241–260. [CrossRef]
39. Kósik, S.; Rees, C.; Palmer, A.S.; Todd, M.; Tost, M.; McKay, W. From sink to source: Late Quaternary landscape evolution and fluvial dynamics of the Hautapu River catchment, New Zealand. *Geomorphology* **2022**, *412*, 108319. [CrossRef]
40. Land Information New Zealand (LINZ). Manawatū–Whanganui LiDAR 1 m DEM. 2024. Available online: https://data.linz.govt.nz/layer/120816-manawatu-whanganui-lidar-1m-dem-2024/ (accessed on 5 March 2026).
41. Wilson, J.P.; Gallant, J.C. (Eds.) *Terrain Analysis: Principles and Applications*; John Wiley & Sons: New York, NY, USA, 2000.
42. Albani, M.; Klinkenberg, B.; Andison, D.W.; Kimmins, J.P. The choice of window size in approximating topographic surfaces from digital elevation models. *Int. J. Geogr. Inf. Sci.* **2004**, *18*, 577–593. [CrossRef]
43. Sidle, R.C.; Pearce, A.J.; O'Loughlin, C.L. *Hillslope Stability and Land Use*; American Geophysical Union: Washington, DC, USA, 1985.
44. Montgomery, D.R.; Dietrich, W.E. A physically based model for the topographic control on shallow landsliding. *Water Resour. Res.* **1994**, *30*, 1153–1171. [CrossRef]
45. Guzzetti, F.; Mondini, A.C.; Cardinali, M.; Fiorucci, F.; Santangelo, M.; Chang, K.T. Landslide inventory maps: New tools for an old problem. *Earth-Sci. Rev.* **2012**, *112*, 42–66. [CrossRef]
46. Ministry for the Environment (MfE). *Erosion Risk North Island (ERNI) Dataset*; Ministry for the Environment: Wellington, New Zealand, 2012. Available online: https://data.mfe.govt.nz/layer/53177-erosion-risk-north-island-2012/ (accessed on 5 March 2026).
47. Lynn, I.; Manderson, A.; Page, M.; Harmsworth, G.; Eyles, G.; Douglas, G.; Mackay, A.; Newsome, P. *Land Use Capability Survey Handbook: A New Zealand Handbook for the Classification of Land*, 3rd ed.; AgResearch: Hamilton, New Zealand; Landcare Research: Lincoln, New Zealand; GNS Science: Lower Hutt, New Zealand, 2009.
48. Horizons Regional Council. *SLUI Farm-Scale Land Use Capability (LUC) Mapping*; Unpublished GIS Dataset; Horizons Regional Council: Palmerston North, New Zealand.
49. Todd, M. Learnings from ten years of hill country farm plans in the Horizons Region. In *Farm Environmental Planning—Science, Policy and Practice, Proceedings of the Fertilizer and Lime Research Centre Workshop*; Currie, L.D., Christensen, C.L., Eds.; Occasional Report No. 31; Massey University: Palmerston North, New Zealand, 2018; 14p.
50. Morgenstern, R.; Townsend, D.B.; Villamor, P.; Barrell, D.J.A.; Ries, W.F.; Van Dissen, R.J.; Clark, K.J.; Coffey, G.L.; Zoeller, A.; Howell, A.; et al. New Zealand active faults database: The high-resolution dataset v2.0. *N. Z. J. Geol. Geophys.* **2025**, *68*, 955–970. [CrossRef]
51. Kruskal, W.H.; Wallis, W.A. Use of ranks in one-criterion variance analysis. *J. Am. Stat. Assoc.* **1952**, *47*, 583–621. [CrossRef]
52. Dunn, O.J. Multiple comparisons using rank sums. *Technometrics* **1964**, *6*, 241–252. [CrossRef]
53. Jain, A.K. Data clustering: 50 years beyond K-means. *Pattern Recognit. Lett.* **2010**, *31*, 651–666. [CrossRef]
54. Pedregosa, F.; Varoquaux, G.; Gramfort, A.; Michel, V.; Thirion, B.; Grisel, O.; Blondel, M.; Prettenhofer, P.; Weiss, R.; Dubourg, V.; et al. Scikit-learn: Machine learning in Python. *J. Mach. Learn. Res.* **2011**, *12*, 2825–2830.
55. National Institute of Water and Atmospheric Research (NIWA). *River Environment Classification (REC2), Version 5*; NIWA Open Data: Wellington, New Zealand, 2019. Available online: https://data-niwa.opendata.arcgis.com/maps/3a4b6cc2c1c74fbb8ddbe25df28e410c (accessed on 5 March 2026).
56. Strahler, A.N. Dimensional analysis applied to fluvially eroded landforms. *Geol. Soc. Am. Bull.* **1958**, *69*, 279–300. [CrossRef]
57. Heron, D.W. *Geological Map of New Zealand 1:250,000*, 4th ed.; [Digital data]; GNS Science Geological Map Series 1; GNS Science: Lower Hutt, New Zealand, 2023. [CrossRef]
58. Rousseeuw, P.J. Silhouettes: A graphical aid to the interpretation and validation of cluster analysis. *J. Comput. Appl. Math.* **1987**, *20*, 53–65. [CrossRef]
59. Stephens, P.R. Determination of Procedures to Establish Priorities for Erosion Control as Determined in the Southern Ruahine Ranges, New Zealand. Unpublished Master's Thesis, Massey University, Palmerston North, New Zealand, 1975.
60. Pettinga, J.R. Geology and Landslides of the Eastern Te Aute District, Southern Hawke's Bay. Unpublished Ph.D. Thesis, University of Auckland, Auckland, New Zealand, 1980.
61. Crozier, M.J.; McConchie, J.A.; Owen, R.C.; Eyles, R.J. *Mass Movement Erosion, Wairarapa*; Unpublished Report; Department of Geography, Victoria University of Wellington: Wellington, New Zealand, 1982.
62. Grant, P.J. *Recently Increased Erosion and Sediment Transport Rates in the Upper Waipawa River Basin, Ruahine Range, New Zealand*; Soil Conservation Centre Publication No. 5; Ministry of Works and Development: Aokautere, New Zealand, 1983.
63. Marden, M. Geology and Its Relationship to Erosion in the Southern Ruahine Range, North Island, New Zealand. Unpublished Ph.D. Thesis, Massey University, Palmerston North, New Zealand, 1984.

64. Trustrum, N.A.; Thomas, V.J.; Lambert, M.G. Soil slip erosion as a constraint to hill country pasture production. In *Proceedings of the New Zealand Grassland Association*; New Zealand Grassland Association: Mosgiel, New Zealand, 1984; Volume 45, pp. 66–76.
65. Crozier, M.J.; Gage, M.; Pettinga, J.R.; Selby, M.J.; Wasson, R.J. The stability of hillslopes. In *Landforms of New Zealand*, 2nd ed.; Soons, J.M., Selby, M.J., Eds.; Longman Paul Ltd.: Auckland, New Zealand, 1992; pp. 63–90.
66. Keefer, D.K.; Johnson, A.M. *Earth Flows: Morphology, Mobilization, and Movement*; U.S. Geological Survey Professional Paper 1264; U.S. Geological Survey: Washington, DC, USA, 1983.
67. Handwerger, A.L.; Roering, J.J.; Schmidt, D.A.; Rempel, A.W. Kinematics of earthflows in the Northern California Coast Ranges using satellite interferometry. *Geomorphology* **2015**, *246*, 321–333. [CrossRef]
68. Bernard, T.G.; Lague, D.; Steer, P. Beyond 2D landslide inventories and their rollover: Synoptic 3D inventories and volume from repeat LiDAR data. *Earth Surf. Dyn.* **2021**, *9*, 1013–1044. [CrossRef]
69. Henriques, C.; Zêzere, J.L.; Marques, F. The role of the lithological setting on the landslide pattern and distribution. *Eng. Geol.* **2015**, *189*, 17–31. [CrossRef]
70. Mackey, B.H.; Roering, J.J. Sediment yield, spatial characteristics, and the long-term evolution of active earthflows determined from airborne LiDAR and historical aerial photographs, Eel River, California. *Geol. Soc. Am. Bull.* **2011**, *123*, 1560–1576. [CrossRef]
71. Handwerger, A.L.; Roering, J.J.; Schmidt, D.A. Controls on the seasonal deformation of slow-moving landslides. *Earth Planet. Sci. Lett.* **2013**, *377*, 239–247. [CrossRef]
72. Williams, F.; McColl, S.; Fuller, I.; Massey, C.; Smith, H.; Neverman, A. Intersection of fluvial incision and weak geologic structures cause divergence from a universal threshold slope model of landslide occurrence. *Geomorphology* **2021**, *389*, 107795. [CrossRef]
73. Bogaard, T.; Greco, R. Invited perspectives: Hydrological perspectives on precipitation intensity–duration thresholds for landslide initiation: Proposing hydro-meteorological thresholds. *Nat. Hazards Earth Syst. Sci.* **2018**, *18*, 31–39. [CrossRef]
74. Grelle, G.; Revellino, P.; Donnarumma, A.; Guadagno, F.M. Bedding control on landslides: A methodological approach for computer-aided mapping analysis. *Nat. Hazards Earth Syst. Sci.* **2011**, *11*, 1395–1409. [CrossRef]
75. Cellek, S. The effect of aspect on landslide and its relationship with other parameters. In *Landslides*; Zhang, Y., Cheng, Q., Eds.; IntechOpen: London, UK, 2022. [CrossRef]
76. Owen, R.C. Soil strength and microclimate in the distribution of shallow landslides. *J. Hydrol.* **1981**, *20*, 17–26.
77. Hancox, G.T.; Wright, K. *Analysis of Landsliding Caused by the 15–17 February 2004 Rainstorm in the Wanganui–Manawatu Hill Country, Southern North Island, New Zealand*; GNS Science Report 2005/11; Institute of Geological & Nuclear Sciences Limited: Lower Hutt, New Zealand, 2005.
78. Chen, Y.-C.; Chang, K.-T.; Wang, S.-F.; Ho, J.-Y.; Chen, J.-P. Influences of channel–hillslope characteristics on landslide erosion in meandering bedrock rivers. *Catena* **2024**, *245*, 108327. [CrossRef]
79. Fuller, I.C.; Riedler, R.A.; Bell, R.; Marden, M.; Glade, T. Landslide-driven erosion and slope-channel coupling in steep, forested terrain, Ruahine Ranges, New Zealand, 1946–2011. *Catena* **2016**, *142*, 252–268. [CrossRef]
80. Reichenbach, P.; Rossi, M.; Malamud, B.D.; Mihir, M.; Guzzetti, F. A review of statistically based landslide susceptibility models. *Earth-Sci. Rev.* **2018**, *180*, 60–91. [CrossRef]
81. Dymond, J.R.; Ausseil, A.G.; Shepherd, J.D.; Buettner, L. Validation of a region-wide model of landslide susceptibility in the Manawatu–Wanganui region of New Zealand. *Geomorphology* **2006**, *74*, 70–79. [CrossRef]

Disclaimer/Publisher's Note: The statements, opinions and data contained in all publications are solely those of the individual author(s) and contributor(s) and not of MDPI and/or the editor(s). MDPI and/or the editor(s) disclaim responsibility for any injury to people or property resulting from any ideas, methods, instructions or products referred to in the content.